Low-temperature energy conversion using a phase-change acoustic heat engine

Avishai Meir[1], Avshalom Offner[1], Guy Z. Ramon*

Nancy and Stephen Grand Technion Energy Program and Department of Civil & Environmental Engineering, Technion - Israel Institute of Technology, Haifa 32000, Israel

HIGHLIGHTS

- Modified thermoacoustic engine can recover heat at temperatures < 100 °C.
- A condensable vapor is added to the working fluid, improving engine performance.
- The engine operates at temperature differences as low as 30 K.
- Acoustic work increases by as much as a factor of 8.

ARTICLE INFO

ABSTRACT

Low-temperature heat is abundant, accessible through solar collectors or as waste heat from a large variety of sources. Thermoacoustic engines convert heat to acoustic work, and are simple, robust devices, potentially containing no moving parts. Currently, such devices generally require high temperatures to operate efficiently and with high power densities. Here, we present a thermoacoustic engine that converts heat to acoustic work at temperature gradients as low as ∼4–5 K/cm, corresponding with a hot-side temperature of ∼50 °C. The system is based on a typical standing-wave design, but the working cycle is modified to include mass transfer, via evaporation and condensation, from a solid surface to the gas mixture sustaining the acoustic field. This introduces a mode of isothermal heat transfer with the potential of providing increased efficiencies – experiments demonstrate a significant reduction in the operating temperature difference, which may be as low as 30 K, and increased output – this 'wet' system produces up to 8 times more power than its dry equivalent. Furthermore, a simplified model is formulated and corresponds quite well with experimental observations and offering insight into the underlying mechanism as well as projections for the potential performance of other mixtures. Our results illustrate the potential of such devices for harvesting energy from low-temperature heat sources. The acoustic power may be converted to electricity or, in a reverse cycle, produce cooling – providing a potential path towards solar heat-driven air conditioners.

1. Introduction

Low-temperature heat, abundantly available as solar radiation or industrial exhaust streams, is still a largely underutilized energy source. For example, the US manufacturing sector rejects approximately 15 GW of technical potential as waste heat every year [1]. However, converting heat to mechanical energy at low temperatures is inherently inefficient, as dictated by thermodynamics. Therefore, energy conversion devices intended for use under these conditions should ideally be designed to be inexpensive and modular, capable of economical implementation in small scale applications, e.g., at the single dwelling.

Within this context, several emerging technological solutions can be considered. Thermoelectric generators offer high reliability, low weight and simplicity, yet its use has been mostly limited to extreme environments due to high material costs. Recent advances have shown potential for cost reduction, but thermal efficiency will likely still be limited to about 20% of Carnot within the next several years [2]. Organic Rankine Cycle (ORC) technology is more mature, and has been widely applied commercially for biomass combustion, industrial waste heat recovery, and geothermal energy. However, downscaling it to the order of several KW currently increases its cost significantly, making it uneconomical for small scale applications [3]. Sorption refrigeration

---

research is currently focused on decreasing system costs and increasing the coefficient of performance, which is typically below 1 for temperatures under 100 °C [4]. Thus, tapping low-temperature heat, particularly at small scales, remains an important, as yet unresolved, engineering challenge.

Thermoacoustic engines are energy conversion devices, in which pressure oscillations within an acoustic field mediate heat flow and work production. These devices are unique in that they contain no moving mechanical parts or exotic materials, consequently exhibiting great potential for reliability and low-cost [5]. The acoustic power produced using heat, may then be converted into electricity or used in a reversed cycle, for cooling [5]. Thermoacoustic engines were first developed in a standing-wave configuration, which, while simple and straightforward, is characterized by an inherent irreversibility associated with the imperfect thermal contact between gas and solid, necessary for the engine's operation [6]. The greatest breakthrough, to date, has been the realization of a travelling-wave configuration, with a significantly improved efficiency [7]. This configuration has since been developed, and devices with a power output greater than 1 kW have been reported [8,9]. These devices, however, typically operate at high temperatures (> 550 °C), and suffer from considerable losses in the regenerator [10]. Recent designs have been shown to operate at relatively low temperatures of 100–200 °C [11]; however, at such low temperatures the power density drops substantially. Hence, further improvement is required, if low-temperature operation is to be accomplished effectively.

The presence of a condensable vapor on the solid, porous substrate (the 'stack') can offer potential improvements over the 'classical' thermoacoustic cycle. A 'classical' thermoacoustic instability relies on heat conduction between the working fluid (gas) and the solid [5]. In the system reported here, the cycle is augmented with mass transfer (a conceptualization of the mechanism is shown in Fig. 1). When the gas is displaced and compressed, and dependent on the local equilibrium between the gas and liquid, mass is transferred. If the gas partial pressure is lower than the equilibrium value, mass will be released into the mixture – as in the power stroke of an engine. During the expansion stage, mass will be deposited, despite the lowered pressure, if dictated by the local equilibrium (due to a lower ambient temperature, for

example). Heat may still be exchanged in the process by the conductive mode but, more importantly, so is the latent heat of the phase-change process, which can be far greater. Raspet et al. [12] showed theoretically that in such a configuration, pressure oscillations may be triggered at reduced temperatures, due to the altered nature of heat transfer between the gas and solid, now governed by phase change rather than conduction. The same theoretical conclusion was recently realized by Yasui and Izu [13] by applying classical thermoacoustic linear theory in a Lagrangian simulation of a single humid air parcel. These ideas were experimentally demonstrated in recent years by Noda and Ueda [14], who demonstrated the phenomenon on a thermoacoustic engine powered by vaporized water and ethanol, and Kawaminami et al. [15] who improved this evaporator engine by changing the resonator geometry. Tsuda and Ueda have shown that at a certain humidity rate, the temperature of acoustic onset is abruptly reduced, remaining constant for any higher humidity value [16] and also measured the temperature gradient required to initiate self-sustained oscillations in standing and travelling-wave acoustic configurations with a wetted stack, as opposed to the previous evaporator-type designs [17]. Nevertheless, acoustic oscillations in this wetted-stack configuration could not be maintained due to the loss of water to evaporation, while it is still not clear how to recirculate the water without flooding the stack in higher powered evaporator-type engines.

Herein, we report the first successful steady operation of an acoustic engine exhibiting augmented performance due to the presence of evaporation and condensation, in a closed system with a wetted stack and fluid regeneration. In the studied configuration, the repeated phase change of water at the surface of the stack, and resultant improved solid-gas heat exchange, allow it to simultaneously reduce the required temperature gradient and increase the power density, thus addressing two significant drawbacks of current systems. While we also measure the conditions leading to onset of oscillations, as recently reported by Tsuda and Ueda [17], the main step forward performed in the current study is the ability to assess the real power output of steady operation, compared with an identical system where phase-change is absent. Our engine demonstrates a significant reduction, by a factor of 2–3, of the temperature differential required to maintain acoustic oscillations, while also increasing the acoustic output. Furthermore, the mechanism
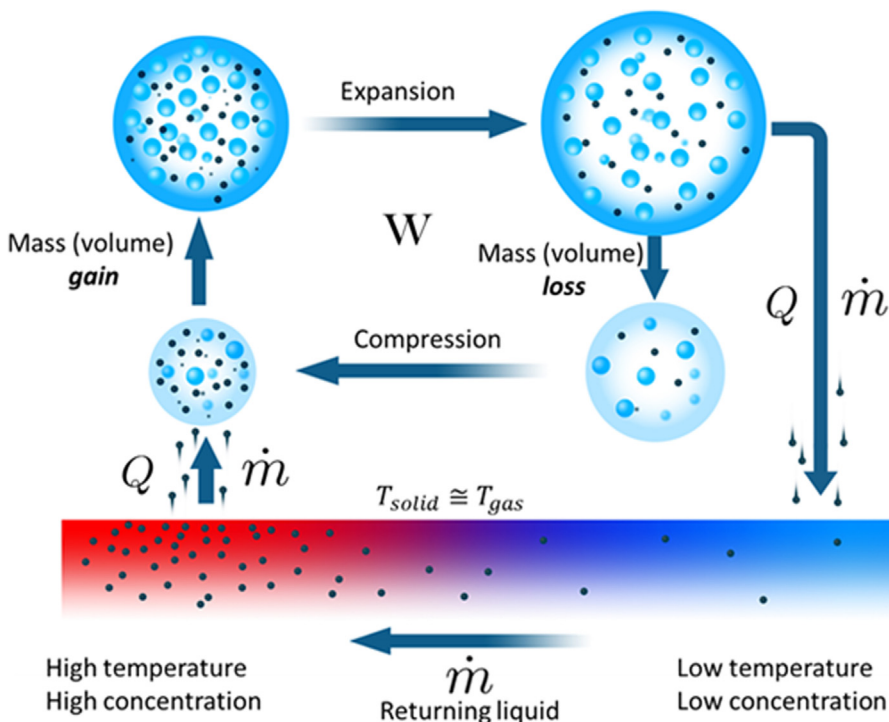
Fig. 1. Conceptualized mechanism of 'phase-change' thermoacoustics. The resonator contains a binary mixture comprising an inert and a 'reactive' component (air and water, respectively, in our experiment) that undergoes reversible sorption with the solid sorbent 'stack' (or, possibly, evaporation/condensation). Gas motion is accompanied by pressure variations that execute a thermodynamic cycle: compression occurs during motion towards the hot end where, due to the heating (using low-temperature solar or waste heat), equilibrium conditions favor desorption and the reactive component is released into the gas mixture, causing it to expand at high pressure – a power stroke. During the second half-cycle, the gas expands as it moves to the cold side, where mass is lost due to sorption, once again performing work on the gas as it contracts at low pressure. This cycle produces acoustic power. In our system, liquid water travels back within the stack walls by capillary action and gravity.
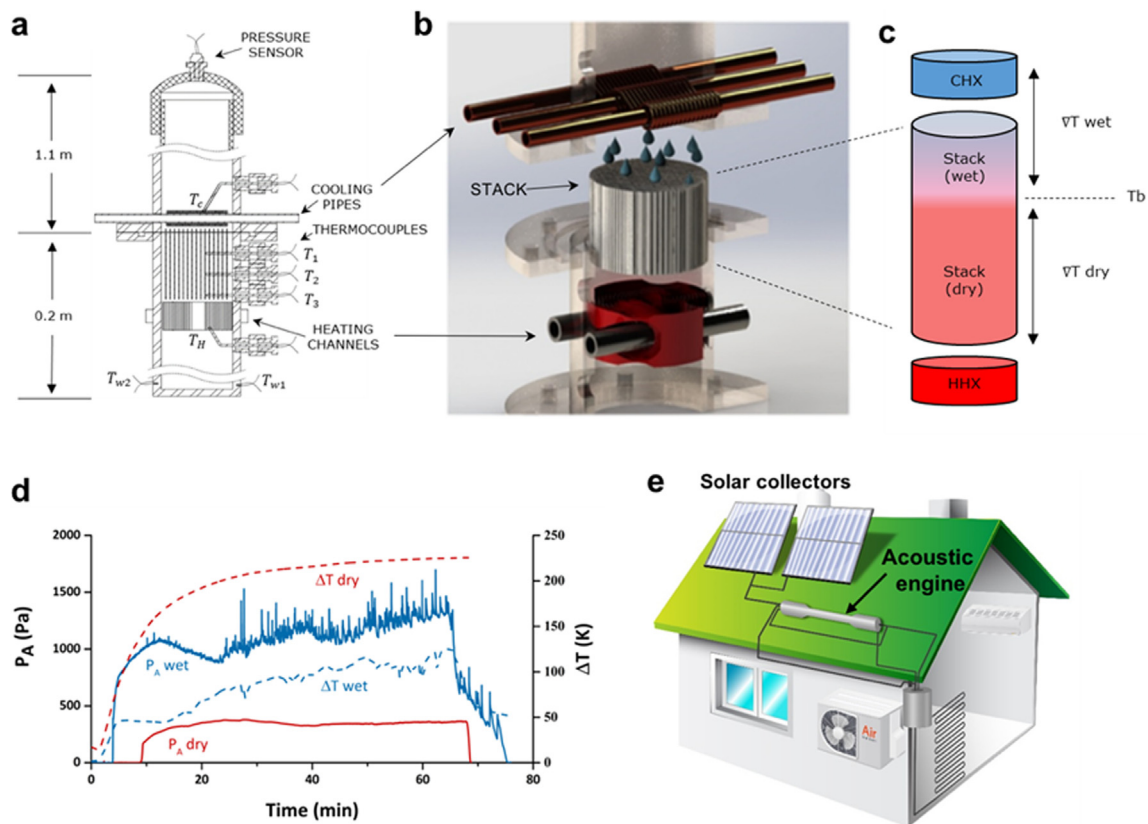
Fig. 2. (a) Schematic drawing of our experimental system, with the locations of the heat exchangers and measurement probes. (b) Expanded view of the 'stack' and heat exchanger in the standing-wave thermoacoustic engine designed for the current study. Water, contained within the porous walls of the ceramic stack, is driven upwards by acoustic mass transfer, where it ultimately condenses on the heat exchanger, and returns back into the stack where it is re-absorbed and evaporated. (c) In our system, as the wet stack is heated, the liquid-water front (where the temperature is 100 °C), is driven closer to the cold heat exchanger, to an extent dictated by the heating power. (d) Comparison of typical, one hour long, wet- and dry-mode experiments, under 90 W of heating. With a wet stack, the engine's steady-state pressure amplitude is significantly higher than with a dry stack under the same heating rate. It is also characterized by a significantly lower temperature difference across the 5 cm stack. (e) Conceptual single-dwelling application of our system: a phase-change thermoacoustic engine can operate at low temperatures, and can thus potentially be used in conjunction with rooftop solar collectors as heat sources. The generated acoustic power can drive cooling or be converted to electricity.

of such operation has been qualitatively captured by a simplified thermodynamic model, facilitating an intuitive understanding of the potential benefits of this design, using various gas-vapor mixtures.

2. Experimental methods

The experimental system is a standing-wave thermoacoustic engine, comprising a sealed tube filled with atmospheric air, with hot and cold heat exchangers sandwiching a ceramic honeycomb 'stack' (see Fig. 2a and 2b for a schematic drawing). The first two sections, which include the hot and cold heat exchangers, were made from 2″ stainless steel pipes, while the subsequent section is a PVC tube with an approximately similar diameter, amounting to a total length of 1.3 m. The system was roughly optimized to suit a 5 cm long, cordierite 'stack' with square channels of ~1 mm height. This was done by positioning the stack 150 mm from the pressure antinode of the generated standing-wave, which is approximately 1/20 of the wavelength at a resonant frequency of about 120 Hz at 1 atm. For these conditions the thermal and mass diffusion penetration depths, representing the distance across which conduction and diffusion occur over one half oscillation period, are $\delta_\alpha, \delta_D \sim 0.3$ mm, respectively (see definitions in supplemental note 3a).

The hot heat exchanger was made from a 0.2 mm-thick, 20 mm-wide stainless steel sheet pressed into a sine-wave shape and rolled to create corrugated channels with a maximum height of ~2 mm [18]. Heating was achieved by inserting two cartridge heaters into stainless

steel tubes drilled into the assembly. The cold heat exchanger was fabricated by inserting three copper pipes through the duct and winding copper wire (1.5 mm diameter) around them. The heat exchanger was cooled by circulating water within the copper pipes, at constant temperature of 20 °C, supplied by a circulating chiller (Thermo Scientific A25). Temperature was measured, via type K thermocouples, on the two heat exchangers and at three locations along the stack, beginning 2 mm from the hot end and then spaced 15 mm from each other. Pressure measurements were obtained using high-sensitivity piezo-electric pressure transducers (Endevco Meggitt 8510B), one inserted at the closed end of the resonator to measure the maximum pressure amplitude, and two others, approximately 200 mm from the cold end of the stack, to measure the acoustic power flux using the two-microphone method [19]. Previous work [20] has demonstrated the accuracy of this method for measuring the acoustic intensity, when compared to the use of direct laser Doppler velocimetry (LDV) measurement. In addition, the pressure transducers' total error band is equivalent to ~200 Pa, which was well within the range of our pressure amplitude measurements.

The experimental procedure begins by soaking the stack in distilled water for 10 min, and then clearing the channels of excess water by blowing air into it. This way, only the pores within the stack wall remained soaked, and the stack was found to repeatedly retain water at ~19–21% of its weight. The stack was then inserted into the system whereupon heating was initialized and maintained at a constant rate for one hour. An array of experiments was performed by changing the

electrical heating power in 20 W increments. The following conditions were set: first, each experiment was repeated three times for the wet stack and twice for the dry stack. More repetitions were performed with the wetted stack since the variability of the acoustic output in its experiments appeared slightly higher than with the dry stack. In our system, water vapor is transported by thermoacoustic mass-streaming [21] towards the cold heat exchanger, where it is condensed, returned by gravity and capillary action back into the stack, to a point where it again evaporates (Fig. 2c). In this manner, a 'wet', two-phase mode of operation is steadily maintained.

A heating power of 190 W was chosen as an upper limit due to some concern that the intense heating would damage the heat exchanger construction and hinder the results. Heating was turned off after 3600 s in the wet mode and 2500 in the dry mode. This condition was chosen following preliminary testing that showed no significant variations in the acoustic output observed in the dry mode after more than 40 min, as illustrated in Fig. 2d.

3. Model formulation

3.1. Acoustic power

The acoustic power, produced as pressure-volume work may be approximated as

$$d\dot{W} = -\omega p dV, \tag{1}$$

where ω is the angular frequency, p is the pressure, and dV is the volumetric change. In a 'dry' system, changes in volume occur via heat transfer driven by local differences in the temperature of the solid and gas, such that $dV \propto dT$ and

$$dT = T_1 - \xi_1 \nabla T_m = T_1(1-\Gamma), \tag{2}$$

where T_1 is the gas temperature perturbation due to adiabatic compression and expansion, ξ_1 is the axial displacement of the gas in the acoustic field, ∇T_m is the temperature gradient imposed on the solid and gas, and $\Gamma = \nabla T_m / \nabla T_g$ is the ratio between the imposed temperature gradient to the gas adiabatic temperature gradient (see supplemental note 1). In a phase-change (or 'wet') system, we assume that changes in volume are the result of evaporation and condensation, driven by local partial pressure differences, between the liquid-soaked wall and the mixture. Hence, $dV \propto d(C_m p)$ and

$$d(C_m p) = C_m p_1 - \xi_1 p_m \nabla C_m = C_m p_1(1-\Gamma_c), \tag{3}$$

where C_m is the vapor concentration, expressed as a mole fraction, p_1 is the pressure oscillation amplitude, ∇C_m is the concentration gradient imposed along the stack, and $\Gamma_c = \nabla C_m / \nabla C_g$, analogous to , is a ratio of the imposed concentration gradient to the adiabatic concentration gradient experienced by the gas as it compresses and expands. Substituting Eqs. (2) and (3) into the general expression of acoustic power (see supplemental note 3b for full derivation) yields expressions for the acoustic power produced by an engine operating in a 'dry' (subscript d) or 'wet' (subscript w) mode,

$$d\dot{W}_d \approx \frac{\omega \Pi \delta_\alpha}{p_m} \frac{\gamma-1}{\gamma} p_1^2 (\Gamma-1) dx \tag{4}$$

$$d\dot{W}_w \approx \frac{\omega \Pi \delta_D}{p_m} C_m p_1^2 (\Gamma_c-1) dx \tag{5}$$

where $\Pi \delta$ is the channel's cross section, with Π denoting the channel width and $\delta_\alpha = \sqrt{2\alpha/\omega}$, $\delta_D = \sqrt{2D/\omega}$ denoting the 'penetration depth' of

heat (α) and mass (D) diffusion, respectively.

3.2. Temperature and concentration gradients

In classical thermoacoustics, a useful definition is $\Gamma = \nabla T_m / \nabla T_g$, the ratio between the ambient temperature gradient, ∇T_m, imposed on the stack, and the adiabatic temperature gradient experienced by the gas, ∇T_g, as it is displaced, due to compression by the sound wave. In a phase-change system, we suggest that the process is driven by a concentration gradient and define an analogous parameter, $\Gamma_c = \nabla C_m / \nabla C_g$, which reflects the ratio of concentration (or partial pressure) variations in the gas, imposed along the stack, and those induced by compression and expansion. In an ideal acoustic engine, this ratio is greater than 1. The two ratios may be related through an equilibrium relation linking the local temperature to the concentration, e.g., the Clausius-Clapeyron equation, here used in the form

$$C_m = exp\left[-\frac{l_h M_r}{R_g}\left(\frac{1}{T_m}-\frac{1}{T_b}\right)\right], \tag{6}$$

where l_h is the latent heat of evaporation, M_r is the vapor molar mass, R_g is the universal gas constant, and T_b is the boiling temperature. ∇C_m and ∇C_g may be written in terms of ∇T_m and ∇T_g, respectively (see supplemental note 2 for full derivation), yielding

$$\Gamma_c = \Lambda \Gamma, \tag{7}$$

in which

$$\Lambda \equiv \frac{l_h}{c_p T_m} \frac{1+\varphi}{1+\varphi C_m}; \quad \varphi \equiv \frac{M_r - M_i}{M_i}, \tag{8}$$

where c_p is the heat capacity at constant pressure, and M_i is the molar mass of the 'inert' gas component. Eq. (8) illustrates that the concentration gradient ratio is smaller than the temperature gradient ratio, since generally $\Lambda > 1$.

3.3. Temperature gradient required for onset of oscillations

In order to further compare the relative performance of the wet and dry mode, we derive a simple expression that relates the respective temperature gradients, considering the acoustic power produced by pressure-volume work executed by the gas oscillations in the two modes – heat or mass-driven, as given by Eqs. (4) and (5). This is accompanied by lost work due to the intrinsic irreversibilities that affect efficiency, namely the imperfect gas-solid thermal and diffusive contact. To derive the expressions for the lost work, we begin with Carnot's efficiency

$$\eta = \frac{\dot{W} + \dot{W}_{lost}}{Q_{in}}, \tag{9}$$

where $\dot{W}_{lost}$ is the work lost due to intrinsic irreversibilities, and Q_{in} is the heat input to the system. For simplicity, and based on experimental observations, we assume the gas in the wet mode remains at approximately the same local temperature as the solid wall, during its oscillatory motion. As such, the wet engine's source of irreversibility is attributed to lateral mass diffusion alone, neglecting conduction. With these assumptions, the resulting expressions for the lost work are as follows (see supplemental note 3A for full derivation):

$$(d\dot{W}_{lost})_d \approx \frac{1}{2}\frac{\omega \delta_\alpha \Pi}{p_m}\frac{\gamma-1}{\gamma} p_1^2 dx, \tag{10}$$

$$(d\dot{W}_{lost})_w \approx \frac{1}{2}\frac{\omega\delta_D\Pi}{p_m}C_m p_1^2 dx, \tag{11}$$

$$\phi_s \equiv \frac{(d\dot{W}_{lost})_d}{(d\dot{W}_{lost})_w} = \left(\frac{D}{\alpha}\right)^{\frac{1}{2}}\frac{C_m}{\frac{(\gamma-1)}{\gamma}}, \tag{12}$$

where γ and α are the ratio of specific heats and thermal diffusivity of the inert gas, respectively. Here, ϕ_s represents the ratio of irreversibilities in the dry and wet modes, and is a key parameter for comparing engine performance between the modes. In an attempt to derive a simple analytical expression, we assume that the heat input to the engine, Q, in both modes of operation is equal at onset (see supplemental note 3C). Under this assumption, we may write

$$\frac{\dot{W}_d + (\dot{W}_{lost})_d}{\eta_d} = \frac{\dot{W}_w + (\dot{W}_{lost})_w}{\eta_w}. \tag{13}$$

Integrating Eqs. (4), (5), (10), and (11) over the stack length (more appropriately, over the temperature range on the stack), we obtain

$$\Gamma_w \approx \frac{1}{\Lambda\phi_s}\frac{\eta_w}{\eta_d}\Gamma_d + \frac{1}{2\Lambda\phi_s}\left(\phi_s - \frac{\eta_w}{\eta_d}\right). \tag{14}$$

Since the term $\phi_s - \eta_w/\eta_d$ is typically very small, this expression may

be further simplified to

$$\Gamma_w \approx \frac{1}{\Lambda\phi_s}\frac{\eta_w}{\eta_d}\Gamma_d. \tag{15}$$

The wet system will therefore require significantly lower temperature gradients at onset, when the term $(\Lambda\phi_s)^{-1}$ is large, reflecting an interplay between losses due to irreversibilities, and gains due to mixture properties. Based on Eq. (15) we expect that, for a given set of conditions and mixture properties, a smaller slope in a Γ_w vs. Γ_d plot represents a system capable of operating at a lower temperature difference. This is an important characteristic of the proposed phase-change mode, and a useful representation for the purpose of comparing different systems.

4. Results and discussion

4.1. Onset and steady operation

Experimental results illustrate some striking differences between the operation of the acoustic engine in which phase-change occurs (a 'wet' engine) compared to that of a 'dry' system (Fig. 3). First, onset of pressure oscillations occurs as the stack average temperature gradient
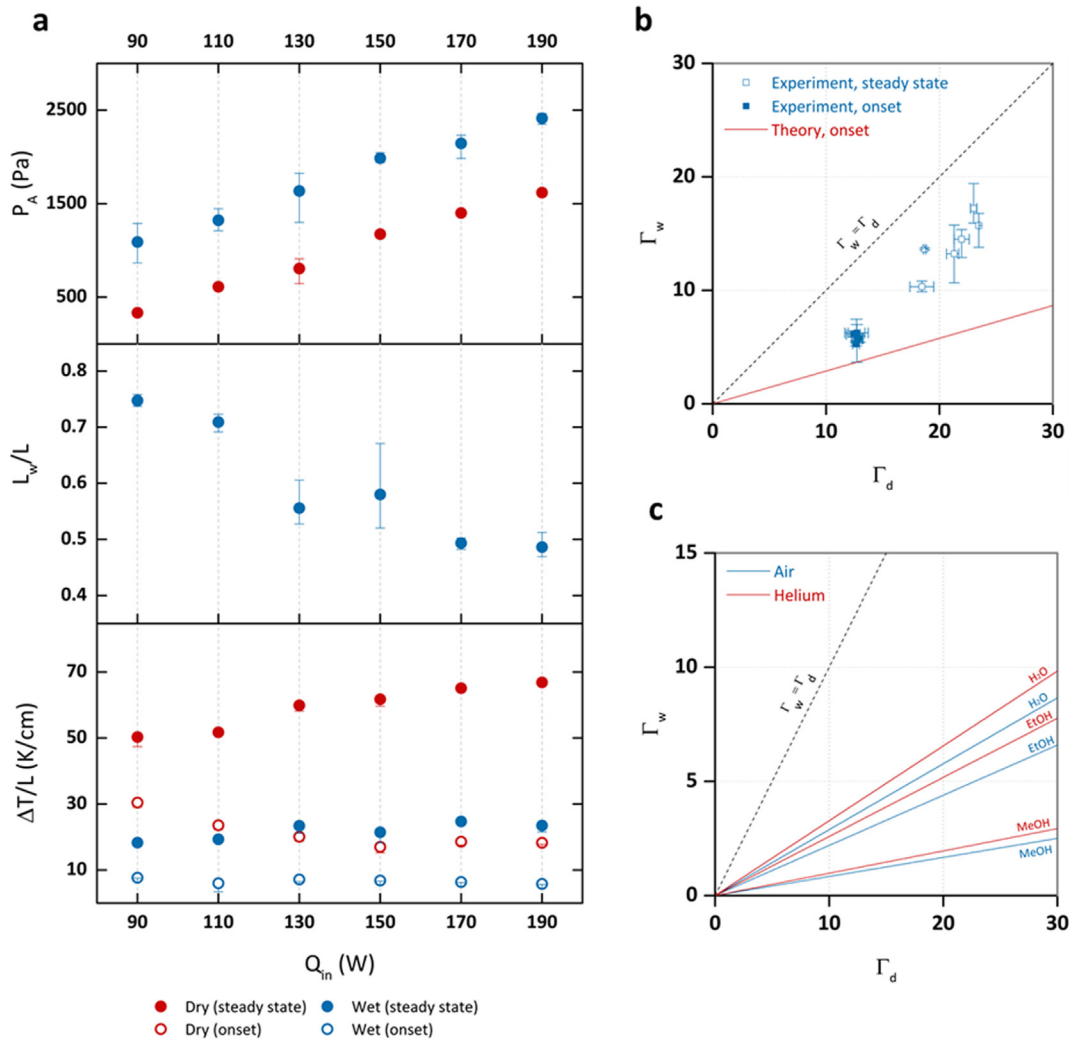
Fig. 3. (a) top panel – the maximum, 15-minute average pressure amplitude, P_A, measured at the resonator end; middle panel – the estimated length of the 'wetted' stack section (below 100 °C) under steady-state operation, Ls, normalized by the total length of the stack, L; bottom panel – the average temperature gradient across the stack during onset and under steady-state operation. The wet-mode temperature gradient is presented for the wetted section of the stack only. (b) Experimental results for the onset and steady-state values of Γ, the ratio of the actual temperature gradient to the adiabatic gradient, in the dry and wet modes. Also shown is a theoretical curve calculated from Eq. (15). (c) Theoretical prediction for Γ at onset, illustrated for several mixtures, calculated by Eq. (15).

reached ~4–5 K/cm (a temperature differential of ~20–25°), as opposed to ~20 K/cm with the dry stack. This reduced onset temperature was recently reported [17], showing similar values. The lower temperature gradient in the wet mode also enabled the engine to run steadily under heat inputs as low as 10 W, compared to about 80 W required for operation in the dry mode. Furthermore, following onset, a gradual increase in the temperature of the stack and hot heat exchanger was observed in the dry mode, while in the wet mode the temperature increase was restricted, presumably by the phase-change. Finally, and perhaps most importantly, in our phase-change engine the pressure amplitude was substantially higher than in the dry mode.

Curiously, the pressure amplitude in the wet engine oscillated frequently, possibly due to a rapidly varying amount of liquid water in the stack following water droplet release from the cold heat exchanger, where condensation occurred. Another interesting feature was observed in the wet mode, following shutdown of the heating source, whereupon the pressure oscillations decreased in two consecutive stages, at distinct rates. Initially the pressure amplitude decreased rapidly, in approximately the same rate as the fast shutdown observed for the dry engine. Afterwards, the pressure amplitude began to decrease slowly for about 10 minutes until the final shut down. These two rates of decrease may be explained as the result of the two separate mechanisms of thermoacoustic conversion taking place simultaneously, one in the dry, high temperature section of the stack, and a second in the wet, low temperature-gradient section (Fig. 2c). The wet portion of the stack, shown in Fig. 3a (middle panel), becomes shorter as the heating rate increases. Our estimate of the wetted region is based on the temperature measurements along the stack, and we consider the region where T > 100 °C to be dry since a wetted region would not exceed the water boiling temperature.

Despite the low temperatures characterizing the wet-mode operation, it consistently produced a higher pressure amplitude than in the dry mode (see Fig. 3a, top panel). An interesting feature that appeared in our experiments was the average temperature gradient measured on the wetted solid stack, ~5 K/cm, which is comparable to the average temperature gradient experienced by a gas parcel during its adiabatic compression\expansion as it is displaced in the acoustic field [5]. Under such conditions, heat transfer by conduction from the gas to the solid is negligible since no significant gradients are generated perpendicular to the solid wall - the mechanism that produces self-sustained oscillations in a standing-wave, 'dry' engine. Instead, in the wet mode, heat transfer is facilitated by transverse, diffusive mass transfer as evaporation and condensation are induced by changes in partial pressure (as shown schematically in Fig. 1).

Our experimental results, both at steady-state and onset, lie below the line representing equal temperature gradients in the wet and dry modes, as shown in Fig. 3b (see supplemental note 4 for calculation procedure of the temperature gradients). Note that the larger scatter between steady-state results stems from the fact that at different heating powers, the 'effective' wet stack is of a different length (as shown in Fig. 3a), hence generating a different gradient. Eq. (15), however simplified, produces a reasonable prediction of onset, when compared with our experimental data (see Fig. 3b). As expected, the experimental data falls slightly higher than the theoretical line, due to non-idealities unaccounted for in the theoretical derivation. These losses grow with the pressure amplitude and become larger under steady-state conditions, increasing the deviation from the theory. The increased deviation of the experimental steady-state results from the theoretical curve mainly reflects our inability to theoretically determine the pressure amplitude for the two modes, which we assume equal at onset in order to plot Eq. (15) – a reasonable assumption since at onset the amplitude is close to zero. Nevertheless, the simple model appears to capture the essential features of the mechanism underlying the engine's operation, relating it to physical system properties.

4.2. Acoustic power

The rate of acoustic work production can be evaluated experimentally by measuring the acoustic intensity at a location close to the stack [19]. This measurement can provide the potential output of an alternator, producing electricity, or other load such as a thermoacoustic cooler. Measurements made 20 cm from the stack, at two intermediate heating rates of 130 W and 200 W, are shown in Fig. 4. Consistent with the pressure amplitude measurements shown in Fig. 3a, a significant difference in acoustic intensity is observed between the wet and dry modes, which increases at the lower heat input. The reason for the decreased difference at higher heating powers is likely the partial drying of the stack – at 130 W, the stack remains wetted to a greater extent than at 200 W with a corresponding contribution of the phase-change cycle. Consequently, the wet-mode power output at 200 W is 106 mW, or ~70 W/m², higher than the dry mode (42 mW or ~28 W/m²) by a factor of 2.5, compared with a factor of ~8 under 130 W (~28 vs ~3 W/m²), representing conditions under which the contribution of the wet mode is more significant. The relatively low output of the current experimental setup, compared with other reported systems, is likely due to 2 main issues.

First, power density scales with the mean pressure [22], which is typically > 10 bars in optimized thermoacoustic systems, whereas here atmospheric pressure was used for simplicity. Second, the current setup is not optimized in terms of heat exchanger design, insulation and choice of working gas. Standing-wave engines have been reported with a thermal to acoustic efficiency of 13% relative to the Carnot efficiency [23], while travelling-wave devices have exceeded ~35% of the Carnot efficiency [8]. Conservatively extrapolating the measured output differences between wet and dry operation and at the atmospheric boiling temperature of water, we estimate a potential thermal efficiency of ~5–10% achievable for phase-change thermoacoustic systems operating at low temperatures, which is comparable, for example, to current thermoelectric technology [24].

4.3. Effect of mixture properties

Encouraged by the reasonable agreement of our simple model with the experimental observations, we use the model to gain further insight into the process, beyond our particular experimental setup that involves an air-water mixture. To this end, we compare different gas mixtures and investigate the parameters affecting onset conditions, as well as the projected acoustic power at steady-state. First, Eq. (15) is used to
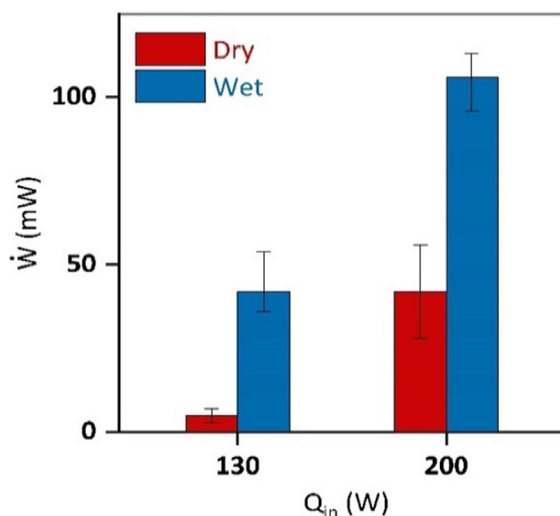
Fig. 4. Work output calculated based on the measured acoustic power 20 cm from the stack. Taking system dimensions into account, the 50 mW mark represents an acoustic intensity of 33 W/m². Error bars represent the range of data.

predict the slope of the wet vs. dry temperature gradients at onset for a few representative mixtures, comprised of two inert components, namely Helium and air, and three reactive components: water, ethanol and methanol (Fig. 3c). The latter two represent condensable species with reduced boiling points, compared with water; however, they also possess lower latent heats of evaporation and varying heat capacities. These interact in a non-trivial manner, conspiring together to dictate the onset conditions for each case. A clear trend is observed; air-based mixtures require a lower gradient, and the temperature gradient at onset trends with the reactive components as $MeOH < EtOH < H_2O$. The difference between He and air can be attributed to the larger critical temperature gradient of He, while it appears that the main characteristic dictating the effect of the reactive component on onset is the vapor-liquid equilibrium that sets the mixture composition, embodied by C_m. Thus, MeOH outperforms water despite its latent heat being roughly half that of water; EtOH, with an even lower latent heat, also requires lower temperature gradients.

Next, we consider general features of mixtures and their impact on the steady operation, particularly the power production (see Fig. 5a). For details of these calculations, please refer to supplemental note 5. Here, we see that the wet system power output increases exponentially with the temperature difference, largely outperforming the dry system. This can, again, be interpreted in light of the vapor-liquid equilibrium curve that exponentially increases the fraction of the reactive component in the mixture, translating to higher power. Further insight can be gained by considering that the power under steady operation (for which $\Gamma \gg 1$), generally scales as $\dot{W} \sim \omega C_m \Lambda \Gamma$ (see Eq. (5) and supplemental note 5), where $C_m \Lambda$ is dependent on mixture properties (specifically, temperature, latent heat, heat capacity, and the molar mass ratio φ) and serves as a 'booster' for the temperature gradient (embodied in Γ). The latent heat represents an energetic potential and the power scales linearly with it, quite intuitively; meanwhile, the heat capacity confines the mixture's ability to produce acoustic work by consuming the energy required for increasing the temperature. Finally, the ratio φ describes the extent to which changes in C_m contribute to the mixture density and pressure, which are essential in producing power. When φ is large, the reactive component, represented by M_r, dominates over the inert component, M_i, and produces a more dramatic influence of phase-change on mixture properties and, hence, power. The resonance frequency, ω, is dependent on system geometry and mixture properties

and is generally proportional to the sound velocity. Fixing the temperature and latent heat, it can be shown that the power scales as $\dot{W} \sim C_m M_i^{1/2}(1 + \varphi)/(1 + \varphi C_m)^{1/2}$ (see supplemental note 6). From this relation we may draw qualitative insight for different molar masses of the reactive and inert components, which illustrates that large values of M_r correspond with increased acoustic power, as does increasing M_i while keeping the ratio φ constant. Furthermore, calculating $C_m \Lambda$ for the different mixtures illustrates the point – insofar as the mixture properties are concerned, operating at lower temperatures largely favors the lower boiling point (MeOH, in our illustration); however, at higher temperatures, the higher latent heat fluid (water, in this case), will offer better potential power output). The temperature range for each mixture is limited by the reactive component's boiling temperature (see Fig. 5b) – the higher the temperature of the mixture, the higher the mole fraction of vapor in the mixture, which increases the relative impact of the compression and, hence, of the phase-change.

5. Concluding remarks

We have experimentally demonstrated how the addition of mass-transfer can significantly and steadily lower the operating temperature range of thermoacoustic engines, and formulated a thermodynamic model capable of explaining the underlying mechanism. A substantial reduction in the temperature gradient required to achieve acoustic onset has been shown and is supported by the simplified model. These calculations and experimental results offer a first step in a path forward towards further developing closed, reliable, thermoacoustic systems that can be used for low temperature heat recovery, without the need for constant vapor supply. Although the work output of a wet stack in our experimental setup was consistently higher than its dry counterpart, there is a measure of uncertainty due to undetermined heat losses caused by insufficient insulation. Nevertheless, the results show that a phase-change engine can be run under very low heat fluxes, in addition to the low temperatures, and offers a significant potential when considering real-world systems operated with waste heat at a constant temperature. Thermoacoustic systems, drawing upon rooftop solar heat collectors, are environmentally benign and can offer a potentially cheap and robust pathway to electricity production and cooling, in the developed and developing world alike, including off-grid locations, with the potential to transform the energy budget on a single dwelling scale.
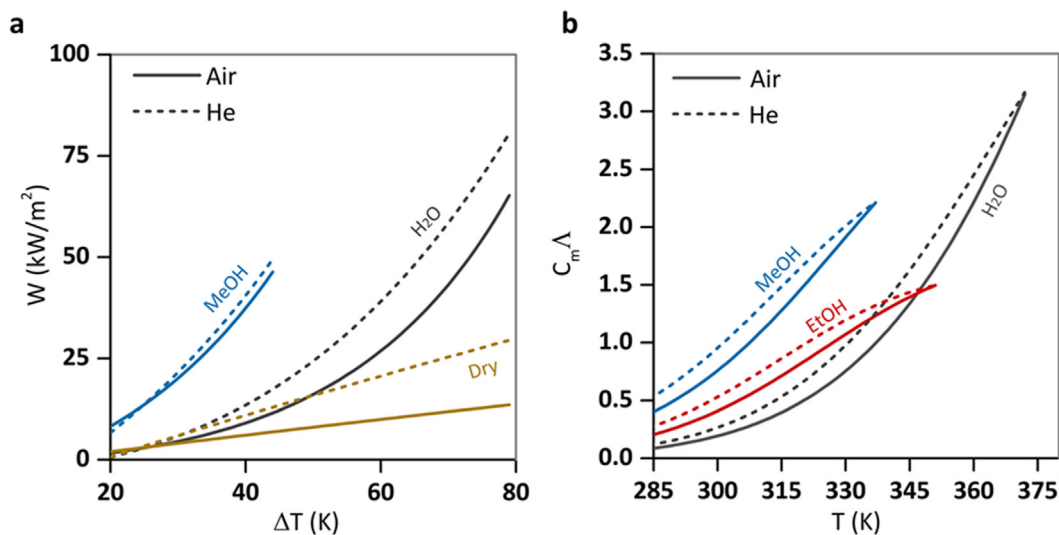
Fig. 5. (a) Acoustic output calculated for mixtures of helium and air in the wet and dry mode (with water and Methanol acting as the condensable species). (b) Values for $C_m \Lambda$, which is proportional to the acoustic work output, shown for various gas mixtures at $p_m = 1$ bar. For details of the calculations, see supplemental note 5.

Acknowledgements

Appendix A. Supplementary material

Supplementary data to this article can be found online at https://doi.org/10.1016/j.apenergy.2018.09.124.

References

[1] Oak Ridge National Laboratory. Waste Heat to Power Market Assessment; 2015.
[2] Champier D. Thermoelectric generators: a review of applications. Energy Convers Manag 2017;140:167–81. https://doi.org/10.1016/j.enconman.2017.02.070.
[3] Quoilin S, Van Den Broek M, Declaye S, Dewallef P, Lemort V. Techno-economic survey of organic rankine cycle (ORC) systems. Renew Sustain Energy Rev 2013;22:168–86. https://doi.org/10.1016/j.rser.2013.01.028.
[4] Cabeza LF, Solé A, Barreneche C. Review on sorption materials and technologies for heat pumps and thermal energy storage. Renew Energy 2017;110:3–39. https://doi.org/10.1016/j.renene.2016.09.059.
[5] Swift GW. Thermoacoustic engines. J Acoust Soc Am 1988;84:1145. https://doi.org/10.1109/ULTSYM.1991.234265.
[6] Wheatley J, Hofler T, Swift GW, Migliori A. An intrinsically irreversible thermoacoustic heat engine. J Acoust Soc Am 1983;74:153–70. https://doi.org/10.1103/PhysRevLett. 50.499.
[7] Backhaus S, Swift G. A thermoacoustic Stirling heat engine. Nature 1999;399:335–8. https://doi.org/10.1038/20624.
[8] Bi T, Wu Z, Zhang L, Yu G, Luo E, Dai W. Development of a 5 kW traveling-wave thermoacoustic electric generator. Appl Energy 2017;185:1355–61. https://doi.org/10.1016/j.apenergy.2015.12.034.
[9] Wu Z, Zhang L, Dai W, Luo E. Investigation on a 1 kW traveling-wave thermoacoustic electrical generator. Appl Energy 2014;124:140–7. https://doi.org/10.1016/j.apenergy.2014.02.063.
[10] Backhaus S, Swift GW. A thermoacoustic-Stirling heat engine: detailed study. J Acoust Soc Am 2000;107:3148. https://doi.org/10.1121/1.429343.
[11] Jin T, Yang R, Wang Y, Feng Y, Tang K. Low temperature difference thermoacoustic prime mover with asymmetric multi-stage loop configuration. Sci Rep 2017;7:7665. https://doi.org/10.1038/s41598-017-08124-5.
[12] Raspet R, Slaton WV, Hickey CJ, Hiller RA. Theory of inert gas-condensing vapor thermoacoustics: propagation equation. J Acoust Soc Am 2002;112:1414–22. https://doi.org/10.1121/1.1508114.
[13] Yasui K, Izu N. Effect of evaporation and condensation on a thermoacoustic engine: a Lagrangian simulation approach. J Acoust Soc Am 2017;141:4398–407. https://doi.org/10.1121/1.4985385.
[14] Noda D, Ueda Y. A thermoacoustic oscillator powered by vaporized water and ethanol. Am J Phys 2013;81:124–6. https://doi.org/10.1119/1.4766940.
[15] Kawaminami S, Sakamoto SI, Fukuda S, Watanabe Y. Step-type thermoacoustic system saturated with water vapor: study for stabilization of low-temperature driving. Jpn J Appl Phys 2017;56. https://doi.org/10.7567/JJAP.56.07JE12.
[16] Tsuda K, Ueda Y. Abrupt reduction of the critical temperature difference of a thermoacoustic engine by adding water. AIP Adv 2015;5:097173 https://doi.org/10.1063/1.4932036.
[17] Tsuda K, Ueda Y. Critical temperature of traveling- and standing-wave thermoacoustic engines using a wet regenerator. Appl Energy 2017;196:62–7. https://doi.org/10.1016/j.apenergy.2017.04.004.
[18] Tijani MEH, Zeegers JCH, De Waele ATAM. Construction and performance of a thermoacoustic refrigerator. Cryogenics (Guildf) 2002;42:59–66. https://doi.org/10.1016/S0011-2275(01)00180-1.
[19] Fusco AM, Ward WC, Swift GW. Two-sensor power measurements in lossy ducts. J Acoust Soc Am 1992;91:2229–35. https://doi.org/10.1121/1.403656.
[20] Biwa T, Tashiro Y, Nomura H, Ueda Y, Yazaki T. Experimental verification of a two-sensor acoustic intensity measurement in lossy ducts. J Acoust Soc Am 2008;124:1584–90. https://doi.org/10.1121/1.2953311.
[21] Weltsch O, Offner A, Liberzon D, Ramon GZ. Adsorption-Mediated Mass Streaming in a Standing Acoustic Wave. Phys Rev Lett 2017;118:118.244301. https://doi.org/10.1103/PhysRevLett.118.244301.
[22] Swift GW. Thermoacoustics. Acoustical Society of America; 1999.
[23] Swift GW. Analysis and performance of a large thermoacoustic engine. J Acoust Soc Am 1992;92:1551. https://doi.org/10.1121/1.403896.
[24] Twaha S, Zhu J, Yan Y, Li B. A comprehensive review of thermoelectric technology: materials, applications, modelling and performance improvement. Renew Sustain Energy Rev 2016;65:698–726. https://doi.org/10.1016/j.rser.2016.07.034.